Solving Inverse Problems in Stochastic Self-Organising Systems through Invariant Representations

Elias Najarro[‡]
© 0000-0002-7875-3251
IT University of Copenhagen
2300 Copenhagen, Denmark

Nicolas Bessone[‡]
© 0009-0008-9008-0003
IT University of Copenhagen
2300 Copenhagen, Denmark

Sebastian Risi
© 0000-0003-3607-8400
IT University of Copenhagen
2300 Copenhagen, Denmark

Abstract

Self-organising systems demonstrate how simple local rules can generate complex stochastic patterns. Many natural systems rely on such dynamics, making selforganisation central to understanding natural complexity. A fundamental challenge in modelling such systems is solving the inverse problem: finding the unknown causal parameters from macroscopic observations. This task becomes particularly difficult when observations have a strong stochastic component, yielding diverse yet equivalent patterns. Traditional inverse methods fail in this setting, as pixelwise metrics cannot capture feature similarities between variable outcomes. In this work, we introduce a novel inverse modelling method specifically designed to handle stochasticity in the observable space, leveraging the capacity of visual embeddings to produce robust representations that capture perceptual invariances. By mapping the pattern representations onto an invariant embedding space, we can effectively recover unknown causal parameters without the need for handcrafted objective functions or heuristics. We evaluate the method on two canonical modelsa reaction-diffusion system and an agent-based model of social segregation-and show that it reliably recovers parameters despite stochasticity in the outcomes. We further apply the method to real biological patterns, highlighting its potential as a tool for both theorists and experimentalists to investigate the dynamics underlying complex stochastic pattern formation.

1 Introduction

Complex systems—such as cellular automata, reaction-diffusion, or agent-based models (ABM)—self-organise into complex dynamical patterns driven by simple rules. The conventional modelling approach of complex systems consists in making an educated guess of the local rules, simulating them—be it a partial differential equation, a cellular automaton, or an agent-based model—and observing whether the emergent patterns are compatible with the phenomena we seek to explain. This modelling approach has proven highly successful in providing mechanistic understanding of a variety of phenomena, including early work on social segregation in urban environments [1], sociology [2], financial markets dynamics [3], and ecology [4, 5]. For instance, in the context of morphogenesis [6, 7], Manukyan et al. [8] identified the specific cellular automata rule and the underlying reaction-diffusion process that give rise to the skin patterns present in ocellated lizards.

[‡]Equal contribution.

Inverse modelling formulates the problem in the reverse causal direction: "Given these macroscopic observations, what are the underlying rules that produce them?" [9, 10]. An inverse model takes an observation as input and returns the model, or initial configuration, that generates the observation. See Figure 1 for a visual summary of inverse modelling and some of its difficulties.

A major challenge in inverse problems is the presence of stochasticity in the observations. Natural phenomena, notably those associated with complex systems, exhibit sensitivity to initial conditions. That is, the same model, under slightly different initial conditions, evolves towards divergent patterns [11– 13]. Often, these patterns share high-level features but do not match when compared pixel by pixel. They are stochastic instances of the same class of patterns; see Figure 2 for an example of stochastic patterns in self-organising systems. For instance, while every human fingerprint is unique, they all share characteristic features that make them recognisable as fingerprints. Similarly, no two leopards have identical spot motifs, yet all are immediately identifiable as leopard patterns. In mathematical terms, patterns can belong to the same class in the presence of invariances-be it translational, rotational, etc.

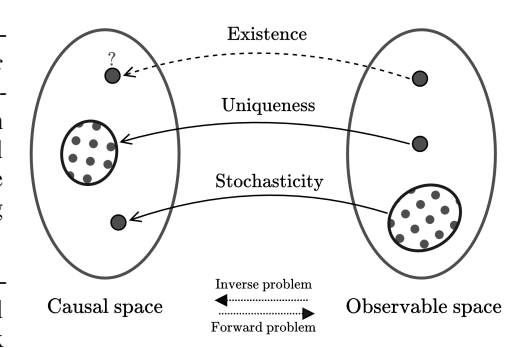


Figure 1: **Inverse problem diagram**. Inverse modelling consists in finding the mapping from observations to their causal space (also referred to as *parameter space*, *solution space* or *domain space* in the literature). It presents several challenges: (i) solutions may not exist for all observations; (ii) the problem of uniqueness: multiple causes may produce identical observations; and (iii) observations may be stochastic, resulting in different observed patterns for the same model parameters. Our method seeks to address the challenge of stochasticity in the observable space.

In this work, we introduce a method that addresses the challenge of solving inverse problems in systems with stochastic observable patterns. The method operates by mapping target patterns onto an invariant embedding representation, enabling the recovery of inverse parameters in stochastic self-organising systems without the need for heuristics or hand-crafted loss functions.

Contributions ① *Conceptually*, we introduce a method for solving inverse problems in stochastic self-organising systems by leveraging visual embedding models to generate invariant representations of observable patterns. To the best of our knowledge, this is the first such approach where stochasticity occurs in the observable rather than the causal space. ② *Technically*, we develop an optimisation framework that combines evolutionary strategies with pre-trained embedding models to address these types of inverse problems. ③ *Empirically*, we evaluate our method on two distinct systems: a chemical reaction-diffusion process and an agent-based model of social segregation. Results show that geometric invariances captured by embeddings can be effectively used to overcome the challenges posed by stochasticity in the observable space.

2 Background

Self-organising systems Self-organisation, understood as the spontaneous emergence of global order or coordination in a system from local interactions of its parts, is observed across different physical, biological, and social systems [14–16]. Examples range from morphogenesis, where cells divide and specialise to form complex body plans in living organisms [17, 18], to animal skin patterns Murray [12] or flocking birds [19]. In social systems, this phenomenon is demonstrated in ABMs, such as Schelling's segregation model, where simple local rules lead to emergent segregation patterns akin to those observed in cities [1].

Self-organising systems are highly sensitive to initial conditions. This sensitivity results in stochastic emergent patterns. For example, the formation of fingerprints or animal skin patterns is driven by genetic signals, local cellular feedback, and mechanical constraints that result in unique patterns on each individual. Even slight variations in initial conditions can produce vastly different results. This property of complex systems poses a significant challenge to inverse problem-solving methods: it requires defining a loss metric that captures the equivalence of patterns with inherent variability.

Inverse problems Solving an *inverse problem* consists in determining the unknown parameters, or initial conditions, of a system from observations of its outcomes [9]. Contrarily, *forward problems* unambiguously map inputs to outputs using the system model. Formally, solving an inverse problem requires finding $(\theta, s_0) \in \Theta \times S$ such that $F(\theta, s_0) = y_{\text{obs}}$, where $F: \Theta \times S \to Y$ denotes the forward model mapping parameters $\theta \in \Theta$ and initial states $s_0 \in S$ to observed data $y_{\text{obs}} \in Y$. Inverse problems are typically ill-posed, characterised by solution non-uniqueness and sensitivity [20]. These properties link inverse problems to complex systems: small changes in their parameters or initial state can result in divergent outcomes. As such, recovering the causal parameters—i.e., solving the inverse problem—shares similar challenges to ill-posed inverse problems.

Stochasticity can be present in inverse problems in two distinct ways. Stochasticity in the causal space: multiple parameters or initial conditions $(\theta, s_0) \in$ $\Theta \times S$ map to identical or nearly identical observations $y_{\text{obs}} \in Y$, resulting in degenerate solutions and non-uniqueness, i.e., non-injectivity of F. In this case, the unknown quantities in the causal space are distributions. An example is seismic tomography, which uses seismic waves recorded at the surface to reconstruct the Earth's interior. Solutions are nonunique: similar surface measurements can originate from different inner structures. Stochasticity in the observable space: in this case, observations are inherently stochastic. Either resulting from randomness in initial states, such as in reaction-diffusion systems $(y_{\text{obs}} = F(\theta, s_0) \text{ with } s_0 \sim \mathcal{S})$, or from intrinsic stochasticity in the forward model F, as in the asynchronous updates of an agent-based model. See Figure 2. The existing literature on inverse stochastic modelling exclusively focusses on the first case: how to address stochasticity in the causal space [21–26], where similar observations can have different causal origins. On the contrary, the method proposed in this work addresses the challenge of stochasticity in the observable space.

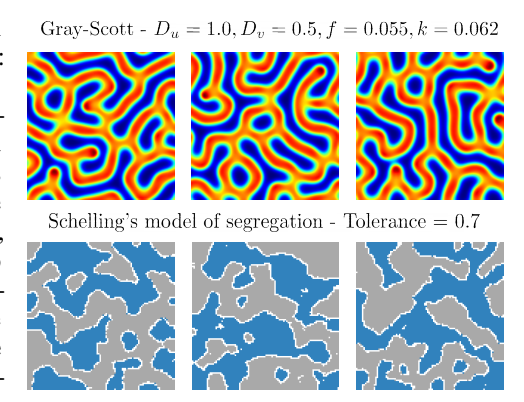


Figure 2: Stochasticity in self-organising systems. Three simulation instances of two self-organising models run with the same parameters. (Top): Reaction-diffusion model; the stochasticity results from varying initial conditions $s_0 \sim \mathcal{S}$. (Bottom): Schelling's model segregation; the stochasticity is present in the model F itself in the form of asynchronous updates. Both systems are examples of stochasticity in the observable space.

Embedding Representations Visual embeddings are learnt vector representations that capture relevant features of images beyond the raw pixel values. Instead of encoding only low-level information, such as colour and intensity, embeddings represent higher-level visual attributes, such as shape, texture, structure, and semantic content [27–31]. Visual embedding models transform image data into a lower-dimensional space where semantically or visually similar images are mapped to nearby points, while dissimilar images are placed farther apart [32–34]. See diagram in Figure 3a.

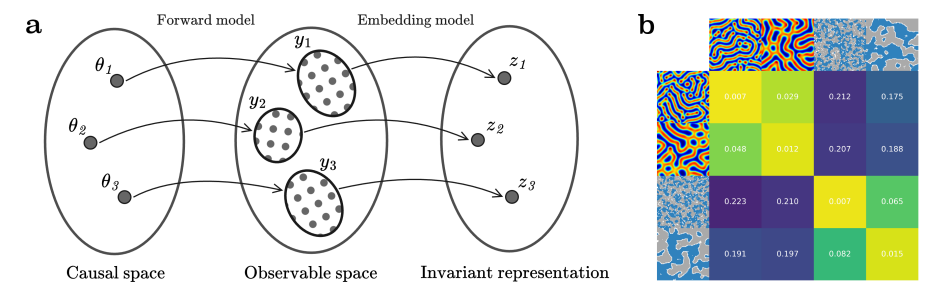


Figure 3: Invariant representations. (a): Diagram representing models parameters θ_i , generating observable patterns y_i , and the visual patterns being mapped to an embedding z_i . (b): Distance matrix between embedding representations z of four patterns (two reaction-diffusion and two ABM segregation patterns). Notice that each of the patterns is an unique instantiation of the models. Similarity clusters appear, suggesting that the embedding model represent patterns with similar features as similar vectors. The values displayed are pairwise cosine distances $1 - \cos(z_i, z_j)$.

Geometric invariant representations. Embedding representations have been shown to be invariant under different pattern transformations [35–38]. For instance, Moskvyak and Maire [32] showed that convolutional embeddings can produce invariant representations of animal patterning under homographic transformations. Our method uses CLIP [33], an open-source vision and text embedding model trained on large-scale datasets using contrastive learning (in this work, only the visual encoder is used). Its embeddings, represented as 512-dimensional vectors, capture high-level visual features. The large variety of images seen by CLIP during training results in rich representations, making them suitable for general-purpose applications without requiring additional fine-tuning. Figure 3b shows that CLIP embeddings are able to capture relevant visual features.

3 Proposed Method

A common approach to solving inverse problems is to formulate them as optimisation problems by defining a loss function that measures the discrepancy between target data and predictions [21, 22]. However, pixel-based metrics are unable to meaningfully capture feature similarities between stochastic patterns. Therefore, they cannot account for the intrinsic variations often present in self-organising patterns. To solve inverse problems with stochasticity in the observable space, a metric capable of capturing the feature-level similarities rather than exact pixel-level matches is needed. Embedding representations offer an effective solution to this challenge by encoding features and invariances of the patterns. The idea behind the proposed method is straightforward: map stochastic patterns onto an embedding space where perceptually similar patterns have similar vector representations. Then, use these invariant representations to solve the inverse problem of finding the unknown parameters that generate the stochastic patterns we seek to reconstruct. A visual summary is provided in Figure 4.

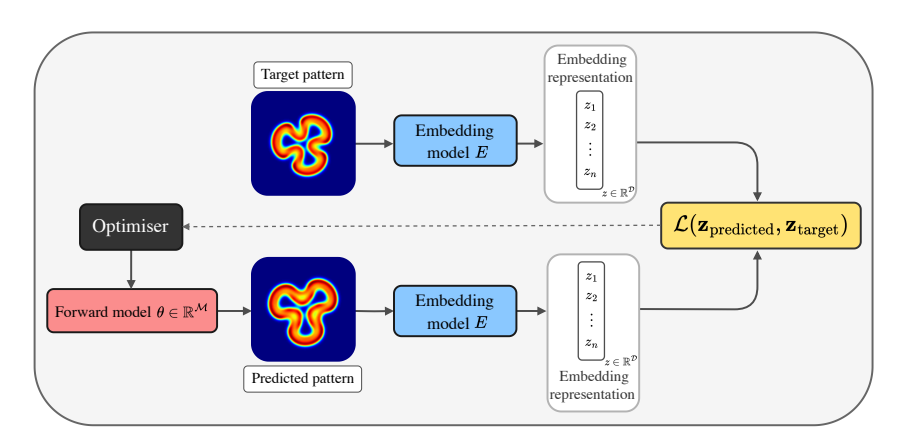


Figure 4: **Method overview.** A target pattern is mapped onto an embedding space $z_{\text{target}} \in \mathbb{R}^{\mathcal{D}}$ using the embedding model E, where D is the embedding space dimension. A forward model, parametrised by $\theta \in \mathbb{R}^{\mathcal{M}}$, where \mathcal{M} is the degrees of freedom of the model, generates a pattern which is mapped to the same embedding space resulting in $z_{\text{predicted}}$. The loss \mathcal{L} between target and predicted embedding guides the optimiser, iteratively updating θ until convergence. By operating in embedding space, the method offers robustness against the inherent stochasticity of emergent patterns.

We demonstrate the method using CLIP, a pre-trained embedding model, to encode the visual patterns into vector embeddings z. Both the target and the predicted patterns are mapped onto the same embedding space, resulting in representations despite stochastic variations. A black-box optimiser is then used to search for the inverse parameters that minimise the embedding distance between the target pattern and the predictions.

We use CMA-ES (Covariance Matrix Adaptation Evolution Strategy), a population-based optimiser [39], to search the causal space. Evolutionary Strategies algorithms have been shown to find high-performing solutions in a variety of tasks [40–42]–including in the context of inverse problems [43, 44]. CMA-ES operates by iteratively updating the covariance matrix of a multivariate normal distribution at each generation, so that candidate solutions θ_i are increasingly guided towards promising

regions of the search space. Solutions are iteratively sampled from a Gaussian distribution centred on the current mean with covariance defining the search distribution: $\boldsymbol{\theta}_i = \mathbf{m} + \Delta \mathbf{C}^{1/2} \sigma$ with $\sigma \sim \mathcal{N}(\mathbf{0}, \mathbf{I})$ where \mathbf{m} is the mean, Δ is the step-size, \mathbf{C} is the covariance matrix and \mathbf{I} is the identity matrix. The mean \mathbf{m} is updated as a weighted sum of selected solutions $\mathbf{m}_{\text{new}} = \sum_{k=1}^{\mu} w_k \boldsymbol{\theta}_k$ where μ is the number of selected solutions, and w_k are the weights based on solution rank. The step-size σ is adjusted to balance exploration and convergence.

The method operates as follows: (1) sample a set of parameters θ_i and random initial states $s_0 \sim \mathcal{S}$, (2) generate the corresponding patterns y_i through the forward model F, (3) use the embedding model to encode the resulting patterns into the embedding space z, (4) compute the loss between the target z_{target} and the candidate solutions, and (5) update the optimiser accordingly. In the case of CLIP, the loss metric is cosine similarity. By focusing on high-level visual similarities rather than pixel-level matches, the method is robust to stochastic variations, and is able to solve inverse problems across entire families of patterns with shared visual features—without requiring handcrafted loss functions. The method is detailed in Algorithm 1.

Algorithm 1 Inverse modelling through embedding representation

```
Require: Forward model F, State space S, Loss function \mathcal{L}, Embedding model E, Optimiser
 1: Choose target pattern y_{target}
 2: while not converged do
          Sample candidate solutions \theta_i from Optimiser
 3:
 4:
          Sample an initial configuration s_0 \in S
          Run simulations: y_{\text{predicted}} \leftarrow F(\theta_i, s_0)
 5:
          Map patterns to embedding space:
 6:
 7:
              z_{\text{target}} \leftarrow E(y_{\text{target}})
              z_{\text{predicted}} \leftarrow E(y_{\text{predicted}})
 8:
          Compute loss: loss_i \leftarrow \mathcal{L}(z_{\text{predicted}}, z_{\text{target}})
 9:
10:
          Update optimiser state with loss_i
11: end while
12: return \theta = \arg\min_{\theta} \log_i
```

The codebase and implementation of the algorithm can be found here: https://github.com/enajx/InverseStochastic.

4 Experiments and Results

In this section, we present the results of applying the method to two self-organising systems: a reaction-diffusion system known as the Gray-Scott model [45, 46], and Schelling's agent-based model of segregation [1]. We chose these two distinct systems, both in terms of scientific domain (biophysical vs. social) and the underlying mathematical model (PDE vs. ABM), to highlight the generality of the method. We first introduce the models, then formulate them as inverse problems, and subsequently present the results of applying the method. Finally, we evaluate the method on two non-simulated patterns: an ocellated lizard and a zebra skin pattern.

Hardware details. Experiments have been run on a single machine with a *AMD Ryzen Threadrip-* per 3990X CPU and a *NVIDIA GeForce RTX 4090* GPU. **Reproducibility.** The experiments can reproduced using the scripts found here: https://github.com/enajx/InverseStochastic/experiments.

4.1 Reaction-Diffusion system

Gray-Scott is a reaction-diffusion model used to study pattern formation in developmental systems [45, 46]. It describes how spatially distributed concentrations of two interacting substances—or morphogens—evolve over time. Morphogens play a critical role in developmental biology by guiding cell differentiation and tissue patterning through their concentration gradients. u represents a nutrient or precursor substance, while v acts as an autocatalyst that promotes its own production while consuming u. The interaction between u and v, combined with their ability to diffuse through space, leads to the emergence of complex patterns such as spots, stripes, or labyrinths. Through this

interplay, the Gray-Scott model provides insights into how local reactions and diffusion contribute to the self-organisation of biological structures. It is formalised as two partial differential equations:

$$\frac{\partial u}{\partial t} = D_u \nabla^2 u - uv^2 + f(1-u) \qquad \text{and } D_v \text{ are the diffusion rates for } u \text{ and } v.$$

$$\frac{\partial v}{\partial t} = D_v \nabla^2 v + uv^2 - (f+k)v \qquad \text{f is the feed rate of } v.$$

$$\cdot f \text{ is the feed rate of } v.$$

$$\cdot k \text{ is the kill rate of } v.$$

- u and v are the chemical concentrations.

- ∇^2 is the Laplacian representing diffusion.

By convention, the u field is treated as a latent variable, while the v field represents the morphogens interpreted as visible patterns.

4.1.1 Results Reaction-Diffusion

In order to find the unknown parameters for the reaction-diffusion system, we follow the algorithm described in Algorithm 1. At each optimisation run, we first generate a target pattern for a set of parameters $\{D_u, D_v, k, f\}_{target} \in \mathbb{R}^4$ by simulating Gray-Scott partial differential equations 4.1 from a random initial state $s_0 \sim S$ for 1000 steps. The resulting pattern is embedded onto z_{target} with the vision model CLIP. z_{target} serves as the target embedding for the loss throughout the optimisation process. Then, the optimiser samples a population of candidate solutions, $\{D_u, D_v, k, f\}_i \in \mathbb{R}^4$, used to simulate the dynamics of reaction-diffusion. The generated patterns y_i are then passed through the embedding model, resulting in z_i . We compare each z_i against the target embedding z_{target} using cosine similarity $cos(z_i, z_{target})$. The optimisation is iteratively run until it converges to a solution that maximises the cosine similarity with respect to the target embedding z_{target} . Results for three sets of reaction-diffusion parameters and its corresponding training curves are shown in Figure 5.

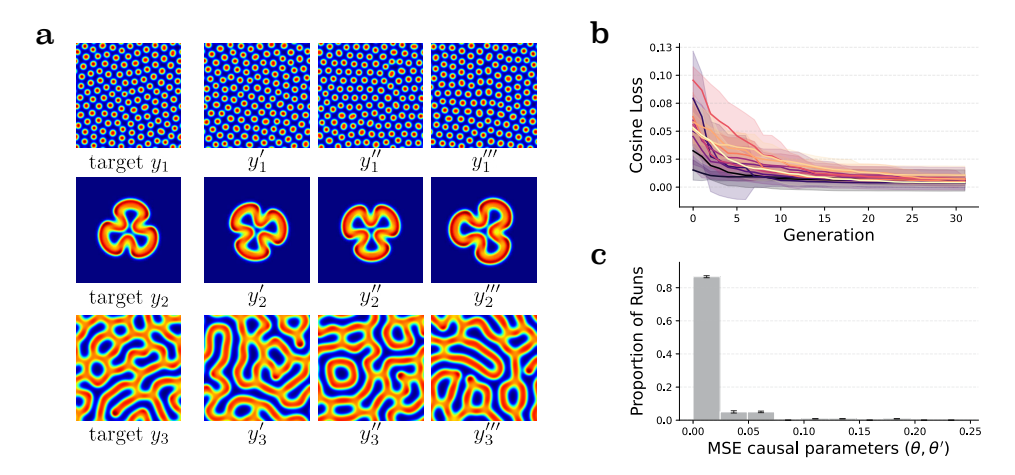


Figure 5: Results for Gray-Scott reaction-diffusion system. (a): A selection of three target patterns y_i (left column), and three reconstructions y_i', y_i'', y_i''' of the causal parameters found by the inverse method on three independent training runs. The method reconstructs patterns with features that qualitatively match the targets. (b): Loss curves showing the average loss and variance of 10 training runs for 12 different patterns. (c): Histogram showing the mean-square errors between the causal θ and predicted parameters θ' ; error bars indicate one standard deviation of the 10 training runs averaged for all the 12 target patterns.

Figure 10 in the Appendix shows the results of 10 independent training runs on a set of 12 target patterns. The loss curves and histogram in Figure 5 reflect results for the full set of twelve target patterns. Figure 12 shows the cosine distance matrix between CLIP embeddings of the set of target patterns used.

4.2 Schelling's Model of Segregation

The second system we use to demonstrate the method is Schelling's segregation model [1], a classic computational model used to study the emergence of spatial patterns in social systems. It illustrates how individual preferences for neighbourhood composition can lead to large-scale segregation, even with mild preferences. This model has been highly influential in computational social science, specifically contributing to the understanding of residential segregation and its implications for urban planning and social dynamics. Schelling's model has a historical significance in computational social science, as it was one of the first to demonstrate how simple local rules can produce complex emergent behaviours, showing the potential of agent-based models to investigate social systems [16, 47]. It is for this latter reason that we chose to demonstrate our method with it.

Our implementation consists of two classes of agents, distributed on a spatial grid. Each agent evaluates its satisfaction based on the proportion of similar neighbours in its local neighbourhood. Unsatisfied agents with their current location will asynchronously relocate to a random location to improve their satisfaction. Schelling's model leads to the emergence of complex segregation patterns that match those observed in urban environments.

$$S_i = \begin{cases} 1 & \text{if } \frac{N_{\text{similar}}}{N_{\text{total}}} \geq T \\ 0 & \text{otherwise} \end{cases}$$

- S_i is the satisfaction of agent i.
- $N_{
 m similar}$ is the number of similar neighbours. $N_{
 m total}$ is the total number of neighbours.
- T is the agent's tolerance threshold, $T \in [0, 1]$.

The emergent patterns, while differing at the microscopic level, exhibit consistent macroscopic structures and statistical properties. It is these invariances of the macroscopic patterns that our method exploits to find the unknown threshold.

4.2.1 Results - Schelling Segregation Model

In this experiment, the same optimisation methodology described in 1 is applied to find the tolerance T from different Schelling segregation patterns. We use a grid size of 100 by 100, and an occupation density of 90%. The results of the experiment are presented in Figure 6.

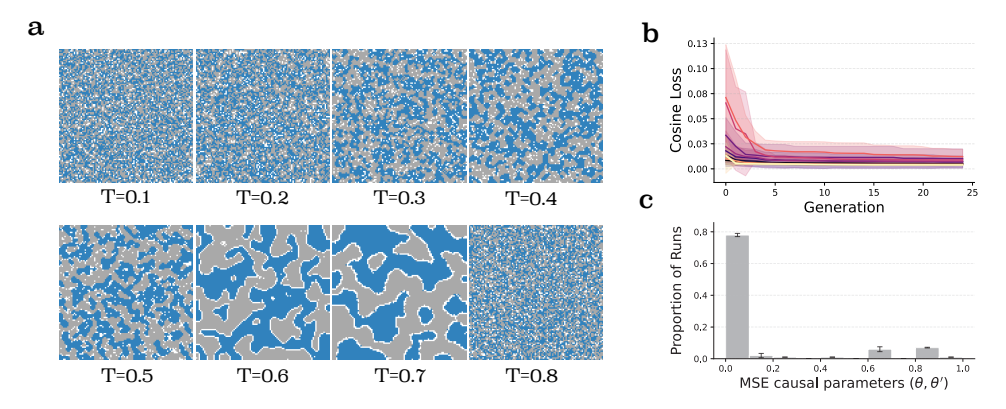


Figure 6: **Results for Schelling segregation model.** (a): Schelling runs with *tolerance* parameter $T \in \{0.1i \mid i \in \{1, 2, \dots, 8\}\}$. For small values of T all agents converges with minimal or no migration since agents are satisfied with diverse neighbours, in middle range of T (3-6) segregation patterns become more pronounced, while for large values of T the system doesn't converge since there are not enough empty cells to allocate all agents under the defined satisfaction threshold. (b): Training curve showing the average loss and variance for target patterns associated to each system tolerance. (c): Histogram showing the mean-square errors between the causal θ and predicted parameters θ' ; error bars indicate one standard deviation of the 10 training runs for each tolerance target.

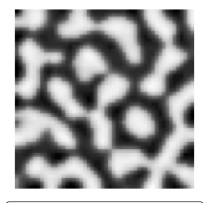
The method successfully finds the inverse parameters. The curves and histogram of Figure 6 indicate the mean and standard deviation of 10 independent training runs. The patterns resulting from each training run are shown in the Appendix, Figure 11. The cosine distance matrix of the CLIP embeddings of the Schelling patterns is shown in the Appendix Figure 13.

4.3 Natural patterns

In this section, we evaluate the method on natural patternsrather than simulated ones, as in the previous experiments. First, on the skin patterning from an ocellated lizard. We provide the method with a target image obtained from Manukyan et al. [8] and search for the unknown parameters of a Gray-Scott reaction-diffusion model to reconstruct the patterns following the same methodology described in 1. The target image and the reconstructed one are shown in Figure 7.

Guiding Model Testing Identifying unknown parameters underlying natural patterns is a significantly more challenging problem as there is no guarantee that the chosen model can generate the target patterns. We often lack an exact model of the underlying process. In such cases, one can approach the problem by including the functional form of the model itself and have the optimiser predict the model's functional form and parameters—an optimisation





Ocellated lizard pattern

Reconstructed pattern

Figure 7: Reconstruction of ocellated **lizard pattern.** Left: Photograph of an ocellated lizard from Manukyan et al. [8], white bar indicates 5mm scale. Right: Reconstructed pattern by the set of reaction-diffusion parameters found by the method. Cosine similarity between target and reconstruction $0.773 \pm$ 0.02, for 100 evaluations.

technique known as symbolic regression [48]. However, the space of possible models is extremely large, and furthermore, we often have an intuition about the model. In such cases, we can conjecture a minimal model form that might be driving the process that generates the target pattern. We can then apply the inverse method to tune the free parameters of the model to reconstruct the natural target. If the model's expressivity is insufficient to capture the pattern, we can iteratively complexify the model. This approach allows us to preserve a mechanistic understanding of the underlying process until the model captures the target pattern.

In this second experiment with natural patterns, we aim at finding the reaction-diffusion parameters that lead to a zebra skin pattern [49]. In our initial attempt at generating a zebra-like pattern, we found that the standard Gray-Scott reaction-diffusion model failed to produce matching results. This suggests that the underlying mechanism responsible for the zebra pattern differs from the assumed model. The Gray-Scott model is isotropic, meaning it treats diffusion equally in all directions, which makes it challenging to generate stripe patterns. To overcome this limitation, we introduced anisotropy into the partial differential equations by allowing the diffusion coefficients to vary directionally:

$$\frac{\partial u}{\partial t} = D_{u_x} \frac{\partial^2 u}{\partial x^2} + D_{u_y} \frac{\partial^2 u}{\partial y^2} - uv^2 + f(1-u)$$
- D_{u_x} and D_{u_y} are the diffusion rates for u in the x - and y -directions.

$$\frac{\partial v}{\partial t} = D_{v_x} \frac{\partial^2 v}{\partial x^2} + D_{v_y} \frac{\partial^2 v}{\partial y^2} + uv^2 - (f+k)v$$
- D_{v_x} and D_{v_y} are the diffusion rates for v in the v - and v -directions.

All other terms remain the same as in the standard Grav-Scott model. This anisotropic modification allows for spatial variation in the diffusion dynamics, introducing a directional bias that can generate the stripe patterns required for the zebra pattern. As a result, the anisotropic Gray-Scott model successfully produces the desired pattern, as shown in Figure 8.

Along with the other approaches discussed in Section 2, the expressivity bottleneck of the model exemplifies how our method can guide the search for mechanistic models. While the method can simply fail due to the optimisation being challenging, by iteratively expanding a conjectured model until it achieves an expressivity level compatible with observed data, we can use the method to potentially identify missing mechanisms and refine our understanding of pattern formation in nature.





Zebra pattern

Reconstructed pattern

Figure 8: Reconstruction of a zebra pattern. Left: Photograph of an zebra skin pattern [49]. Right: Pattern generated by the anisotropic reactiondiffusion model for the parameters found by the method. Cosine similarity between target and reconstruction $0.842 \pm$ 0.018, for 100 evaluations.

5 Conclusion

In this work, we have presented a method for solving inverse problems in stochastic self-organising systems by leveraging invariant visual representations from embedding models—without the need to handcraft metric functions to capture the visual similarities between patterns. The key idea is to shift the optimisation from pixel space to an embedding space where perceptually similar patterns are mapped to nearby points, allowing the recovery of unknown parameters, even those resulting in stochastic patterns. Unlike existing techniques in inverse modelling, the method addresses the issue of stochasticity in the observable space, rather than in the causal space. We have demonstrated the method on two distinct self-organising models: a reaction-diffusion system and an agent-based segregation model, both exhibiting stochasticity in the observation space. For the reaction-diffusion model, we have shown that the approach can be applied to real biological patterns: an ocellated lizard and a zebra skin pattern. Finally, we have illustrated how the framework can guide model testing: when a conjectured model fails to generate the target, it suggests that the model's expressivity is insufficient and extra terms are needed, a practical path for iterative refinement in mechanistic modelling. In summary, the method provides a simple yet effective technique for theorists and experimentalists to investigate and control self-organising stochastic systems.

5.1 Limitations

Embedding capturing the wrong invariances. The embedding representations are only useful to the extent that they are capable of encoding the invariances present in the target patterns. If the embedding model fails to capture the relevant features of the patterns-or encode non-relevant invariances—the optimisation process may converge to parameters that reproduce visually dissimilar results, despite low embedding losses. For example, an embedding might prioritise shape over size, which can lead to false positives in parameter recovery. In other words, the embedding model is capturing an invariance, but might not be an invariance that we want. While this property may be desirable for certain problems, it can pose challenges for others. An example of this issue is illustrated in Fig. 9 where the technique finds a set of parameters that reproduce the target patterns but at a reduced scale.

Difficulty of quantitative evaluation. The method comes with the challenge of quantitatively evaluating its results because evaluating the visual similarity between two patterns

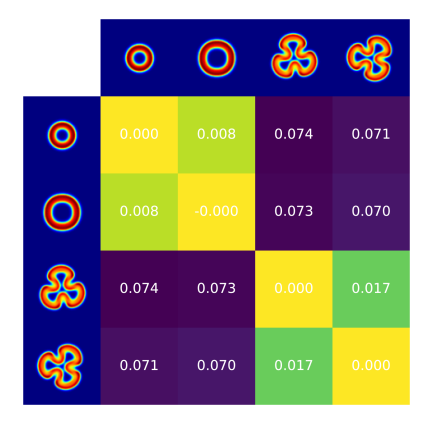


Figure 9: **Embedding invariances.** Distance matrix of four different patterns. CLIP model maps patterns with scale and rotation transformations to similar embedding vectors.

is fundamentally subjective [50]. Visual embedding distances provide a proxy for this, but they do not always match how humans perceive similarity. Often, judging success comes down to visual inspection—you know it when you see it. Although this works in practice, it is inherently subjective. Domain-specific metrics will be needed in order to make the evaluation more systematic.

5.2 Future Work

Domain-specific embedding models. A future path is the use of custom embedding models trained specifically on the types of patterns relevant to the target domain. This could involve fine-tuning or training embedding models—e.g., a variational autoencoder trained on a domain-specific dataset [38]—or augmenting the dataset with relevant transformations for which we want the embedding model to be invariant. This way, the embedding space can be aligned more closely with the visual equivalence classes that matter for the task. Domain-specific embeddings could provide a way of ensuring that the method results in perceptually meaningful reconstructions.

Search on model space When solving an inverse problem, the search space can be the parameters of the forward model $\theta \in \Theta$, the functional form of the model F itself, or the initial configuration $s_0 \in S$ of the system. In this work, we have focused on only the first two cases. A future avenue will be to combine the method with modern symbolic regression techniques [48, 51] to recover the functional forms of the underlying models, and evaluate the method when searching in state space.

References

- [1] Thomas C. Schelling. Dynamic models of segregation. *Journal of Mathematical Sociology*, 1: 143–186, 1971. URL https://api.semanticscholar.org/CorpusID:120637340.
- [2] Federico Bianchi and Flaminio Squazzoni. Agent-based models in sociology. *WIREs Comput. Stat.*, 7(4):284–306, July 2015. ISSN 1939-5108. doi: 10.1002/wics.1356.
- [3] E. Samanidou, E. Zschischang, D. Stauffer, and T. Lux. Agent-based models of financial markets. Rep. Prog. Phys., 70(3):409, February 2007. ISSN 0034-4885. doi: 10.1088/0034-4885/70/3/R03.
- [4] Adam J. McLane, Christina Semeniuk, Gregory J. McDermid, and Danielle J. Marceau. The role of agent-based models in wildlife ecology and management. *Ecol. Model.*, 222(8):1544–1556, April 2011. ISSN 0304-3800. doi: 10.1016/j.ecolmodel.2011.01.020.
- [5] Tatiana Filatova, Peter H. Verburg, Dawn Cassandra Parker, and Carol Ann Stannard. Spatial agent-based models for socio-ecological systems: Challenges and prospects. *Environ. Model. Software*, 45:1–7, July 2013. ISSN 1364-8152. doi: 10.1016/j.envsoft.2013.03.017.
- [6] Eric Bonabeau. From Classical Models of Morphogenesis to Agent-Based Models of Pattern Formation. *Artif. Life*, 3(3):191–211, July 1997. ISSN 1064-5462. doi: 10.1162/artl.1997.3.3. 191.
- [7] Chad M. Glen, Melissa L. Kemp, and Eberhard O. Voit. Agent-based modeling of morphogenetic systems: Advantages and challenges. *PLoS Comput. Biol.*, 15(3):e1006577, March 2019. ISSN 1553-7358. doi: 10.1371/journal.pcbi.1006577.
- [8] Liana Manukyan, Sophie A. Montandon, Anamarija Fofonjka, Stanislav Smirnov, and Michel C. Milinkovitch. A living mesoscopic cellular automaton made of skin scales. *Nature*, 544: 173–179, April 2017. ISSN 1476-4687. doi: 10.1038/nature22031.
- [9] Albert Tarantola. Inverse Problem Theory and Methods for Model Parameter Estimation. Society for Industrial and Applied Mathematics, 2005. ISBN 978-0-89871-572-9 978-0-89871-792-1. doi: 10.1137/1.9780898717921. URL http://epubs.siam.org/doi/book/10.1137/1. 9780898717921.
- [10] Mario Bunge. Inverse problems. Foundations of Science, 24(3):483-525, 2009. ISSN 1572-8471. doi: 10.1007/s10699-018-09577-1. URL https://doi.org/10.1007/s10699-018-09577-1.
- [11] Rick Durrett. Stochastic spatial models. SIAM review, 41(4):677–718, 1999.
- [12] James D Murray. *Mathematical biology: I. An introduction*, volume 17. Springer Science & Business Media, 2007.
- [13] Philip Ball. Shapes: nature's patterns: a tapestry in three parts. OUP Oxford, 2009.
- [14] Hermann Haken. Synergetics: An approach to self-organization. *Self-organizing systems: The emergence of order*, pages 417–434, 1987.
- [15] Stuart A Kauffman. The origins of order: Self-organization and selection in evolution. In *Spin glasses and biology*, pages 61–100. World Scientific, 1992.
- [16] Maya Paczuski and Per Bak. Self-Organization of Complex Systems. *arXiv*, June 1999. doi: 10.48550/arXiv.cond-mat/9906077.
- [17] John Von Neumann, Arthur W Burks, et al. Theory of self-reproducing automata. *IEEE Transactions on Neural Networks*, 5(1):3–14, 1966.
- [18] Paul Weiss and A. C. Taylor. Reconstitution of complete organs from single-cell suspensions of chick embryos in advanced stages of differentiation. *Proc. Natl. Acad. Sci. U.S.A.*, 46(9): 1177–1185, September 1960. doi: 10.1073/pnas.46.9.1177.

- [19] Craig W Reynolds. Flocks, herds and schools: A distributed behavioral model. In *Proceedings* of the 14th annual conference on Computer graphics and interactive techniques, pages 25–34, 1987.
- [20] Charles W. Groetsch. Inverse Problems in the Mathematical Sciences. Vieweg+Teubner Verlag, Wiesbaden, Germany, 1993. ISBN 978-3-322-99202-4. URL https://link.springer.com/ book/10.1007/978-3-322-99202-4.
- [21] Marko Vauhkonen, Tanja Tarvainen, and Timo Lähivaara. Inverse Problems. In *Mathematical Modelling*, pages 207–227. Springer, Cham, Switzerland, July 2016. ISBN 978-3-319-27836-0. doi: 10.1007/978-3-319-27836-0_12.
- [22] Nan Ye, Farbod Roosta-Khorasani, and Tiangang Cui. Optimization Methods for Inverse Problems. In *2017 MATRIX Annals*, pages 121–140. Springer, Cham, Switzerland, March 2019. ISBN 978-3-030-04161-8. doi: 10.1007/978-3-030-04161-8_9.
- [23] Housen Li, Johannes Schwab, Stephan Antholzer, and Markus Haltmeier. Nett: Solving inverse problems with deep neural networks. *Inverse Problems*, 36(6):065005, 2020.
- [24] Bahjat Kawar, Gregory Vaksman, and Michael Elad. Snips: Solving noisy inverse problems stochastically. Advances in Neural Information Processing Systems, 34:21757–21769, 2021.
- [25] Kailai Xu and Eric Darve. Solving inverse problems in stochastic models using deep neural networks and adversarial training. Computer Methods in Applied Mechanics and Engineering, 384:113976, 2021.
- [26] Martin Genzel, Jan Macdonald, and Maximilian März. Solving inverse problems with deep neural networks—robustness included? *IEEE transactions on pattern analysis and machine intelligence*, 45(1):1119–1134, 2022.
- [27] Andrea Frome, Greg S Corrado, Jon Shlens, Samy Bengio, Jeff Dean, Marc'Aurelio Ranzato, and Tomas Mikolov. Devise: A deep visual-semantic embedding model. *Advances in neural information processing systems*, 26, 2013.
- [28] Mohammad Norouzi, Tomas Mikolov, Samy Bengio, Yoram Singer, Jonathon Shlens, Andrea Frome, Greg S Corrado, and Jeffrey Dean. Zero-shot learning by convex combination of semantic embeddings. *arXiv preprint arXiv:1312.5650*, 2013.
- [29] Chao Jia, Yinfei Yang, Ye Xia, Yi-Ting Chen, Zarana Parekh, Hieu Pham, Quoc V. Le, Yunhsuan Sung, Zhen Li, and Tom Duerig. Scaling Up Visual and Vision-Language Representation Learning With Noisy Text Supervision. *arXiv*, February 2021. doi: 10.48550/arXiv.2102.05918.
- [30] Eyvind Niklasson, Alexander Mordvintsev, Ettore Randazzo, and Michael Levin. Self-Organising Textures. *Distill*, 6(2):e00027.003, February 2021. ISSN 2476-0757. doi: 10.23915/distill.00027.003.
- [31] Yingtao Tian and David Ha. Modern Evolution Strategies for Creativity: Fitting Concrete Images and Abstract Concepts. *arXiv*, September 2021. doi: 10.48550/arXiv.2109.08857.
- [32] Olga Moskvyak and Frederic Maire. Learning Geometric Equivalence between Patterns Using Embedding Neural Networks. In 2017 International Conference on Digital Image Computing: Techniques and Applications (DICTA), pages 2017–01. IEEE, 2017. doi: 10.1109/DICTA.2017. 8227457.
- [33] Alec Radford, Jong Wook Kim, Chris Hallacy, Aditya Ramesh, Gabriel Goh, Sandhini Agarwal, Girish Sastry, Amanda Askell, Pamela Mishkin, Jack Clark, Gretchen Krueger, and Ilya Sutskever. Learning Transferable Visual Models From Natural Language Supervision. *arXiv*, February 2021. doi: 10.48550/arXiv.2103.00020.
- [34] Akarsh Kumar, Chris Lu, Louis Kirsch, Yujin Tang, Kenneth O. Stanley, Phillip Isola, and David Ha. Automating the Search for Artificial Life with Foundation Models. *arXiv*, December 2024. doi: 10.48550/arXiv.2412.17799.

- [35] Ian Goodfellow, Honglak Lee, Quoc Le, Andrew Saxe, and Andrew Ng. Measuring invariances in deep networks. *Advances in neural information processing systems*, 22, 2009.
- [36] Zhuotun Zhu, Xinggang Wang, Song Bai, Cong Yao, and Xiang Bai. Deep learning representation using autoencoder for 3d shape retrieval. *Neurocomputing*, 204:41–50, 2016.
- [37] Michael Tschannen, Olivier Bachem, and Mario Lucic. Recent advances in autoencoder-based representation learning. *arXiv preprint arXiv:1812.05069*, 2018.
- [38] Maximilian Ilse, Jakub M Tomczak, Christos Louizos, and Max Welling. Diva: Domain invariant variational autoencoders. In *Medical Imaging with Deep Learning*, pages 322–348. PMLR, 2020.
- [39] N. Hansen and A. Ostermeier. Adapting arbitrary normal mutation distributions in evolution strategies: the covariance matrix adaptation. In *Proceedings of IEEE International Conference on Evolutionary Computation*, pages 312–317. IEEE, May 1996. ISBN 978-0-7803-2902. URL https://ieeexplore.ieee.org/document/542381.
- [40] Luis Miguel Rios and Nikolaos V. Sahinidis. Derivative-free optimization: a review of algorithms and comparison of software implementations. *J. Global Optim.*, 56(3):1247–1293, July 2013. ISSN 1573-2916. doi: 10.1007/s10898-012-9951-y.
- [41] Nacim Belkhir, Johann Dréo, Pierre Savéant, and Marc Schoenauer. Per instance algorithm configuration of CMA-ES with limited budget. In ACM Conferences, pages 681–688. Association for Computing Machinery, New York, NY, USA, July 2017. doi: 10.1145/3071178.3071343.
- [43] Keith C. Bledsoe, Jeffrey A. Favorite, and Tunc Aldemir. Application of the Differential Evolution Method to Solving Inverse Transport Problems. *Nucl. Sci. Eng.*, October 2011. ISSN 1184-1355. URL https://www.tandfonline.com/doi/abs/10.13182/NSE10-28.
- [44] Alexander V. Grayver and Alexey V. Kuvshinov. Exploring equivalence domain in nonlinear inverse problems using Covariance Matrix Adaption Evolution Strategy (CMAES) and random sampling. *Geophys. J. Int.*, 205(2):971–987, May 2016. ISSN 0956-540X. doi: 10.1093/gji/ggw063.
- [45] John E. Pearson. Complex Patterns in a Simple System. Science, 261(5118):189–192, July 1993. ISSN 0036-8075. doi: 10.1126/science.261.5118.189.
- [46] Kyoung J. Lee, W. D. McCormick, Qi Ouyang, and Harry L. Swinney. Pattern Formation by Interacting Chemical Fronts. *Science*, 261(5118):192–194, July 1993. ISSN 0036-8075. doi: 10.1126/science.261.5118.192.
- [47] William AV Clark and Mark Fossett. Understanding the social context of the schelling segregation model. *Proceedings of the National Academy of Sciences*, 105(11):4109–4114, 2008.
- [48] Miles Cranmer. Interpretable machine learning for science with pysr and symbolic regression. jl. *arXiv preprint arXiv:2305.01582*, 2023.
- [49] Emmett Lindner. Last of Escaped Zebras Captured After Being Lured With White Bread. *N.Y. Times*, May 2024. ISSN 0362-4331. URL https://www.nytimes.com/2024/05/04/us/zebra-washington-state-highway-captured.html.
- [50] Mark Wagner. The metric of visual space. Perception & psychophysics, 38:483–495, 1985.
- [51] Silviu-Marian Udrescu and Max Tegmark. AI Feynman: A physics-inspired method for symbolic regression. *Sci. Adv.*, 6(16), April 2020. ISSN 2375-2548. doi: 10.1126/sciadv. aay2631.

6 Appendix

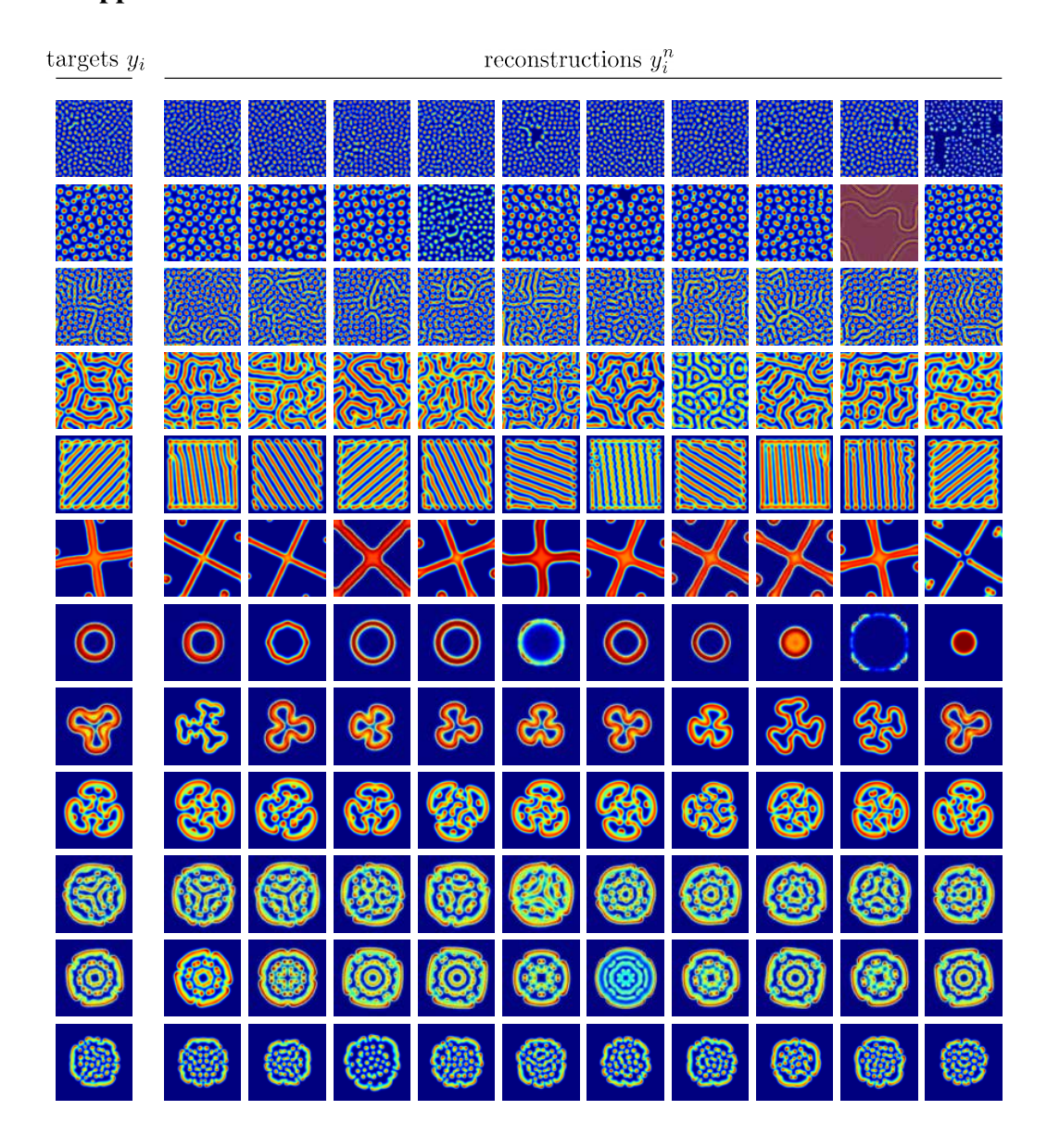


Figure 10: **Results for Gray-Scott model.** Twelve target patterns y_i (left column), each produced by simulating Gray-Scott partial differential equations 4.1 for different parameters θ_i and random initial states s_{0i} . The reconstructions columns show the patterns y_i^n recovered by our method for 10 independent training runs. The corresponding training curves and loss histograms are shown in Figure 5.

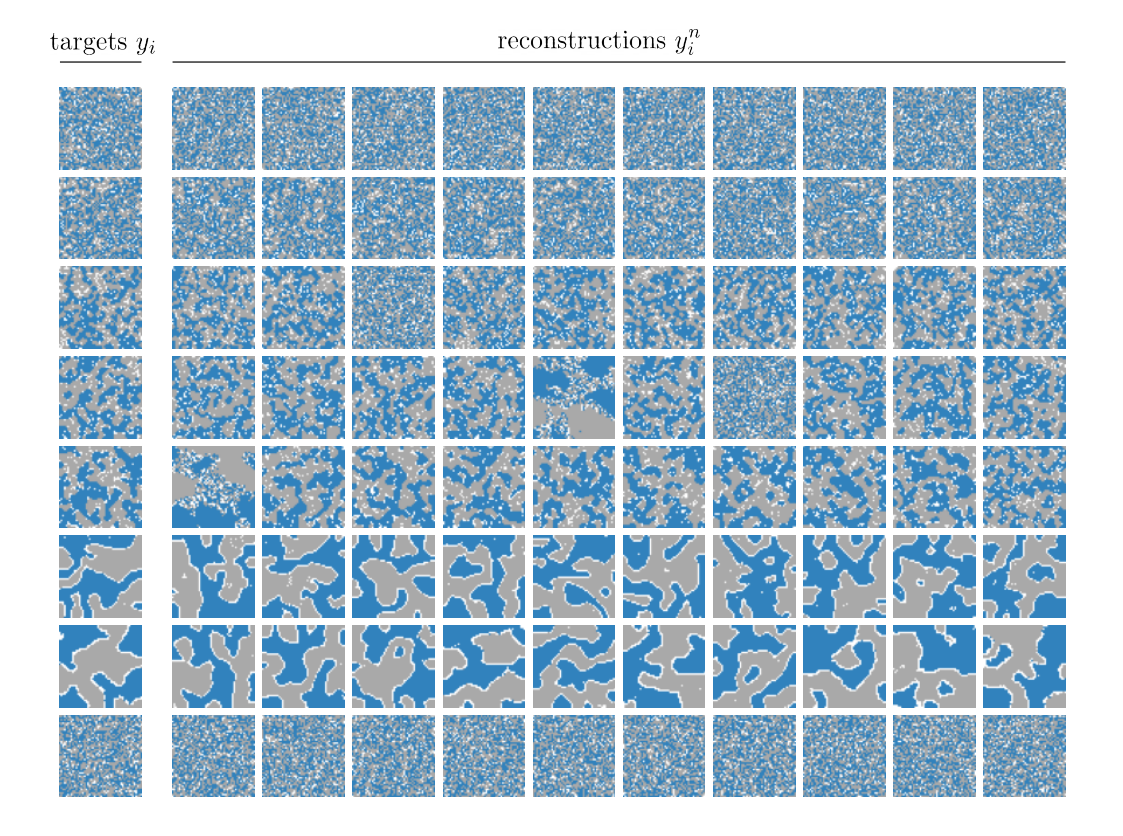


Figure 11: **Results for Schelling's segregation model.** Eight target patterns y_i (left column), each produced by simulating Schelling ABM model of segregation 4.2 for different parameters θ_i and random initial states s_{0i} . The reconstructions columns show the patterns y_i^n recovered by our method for 10 independent training runs. The corresponding training curves and loss histograms are shown in Figure 6.

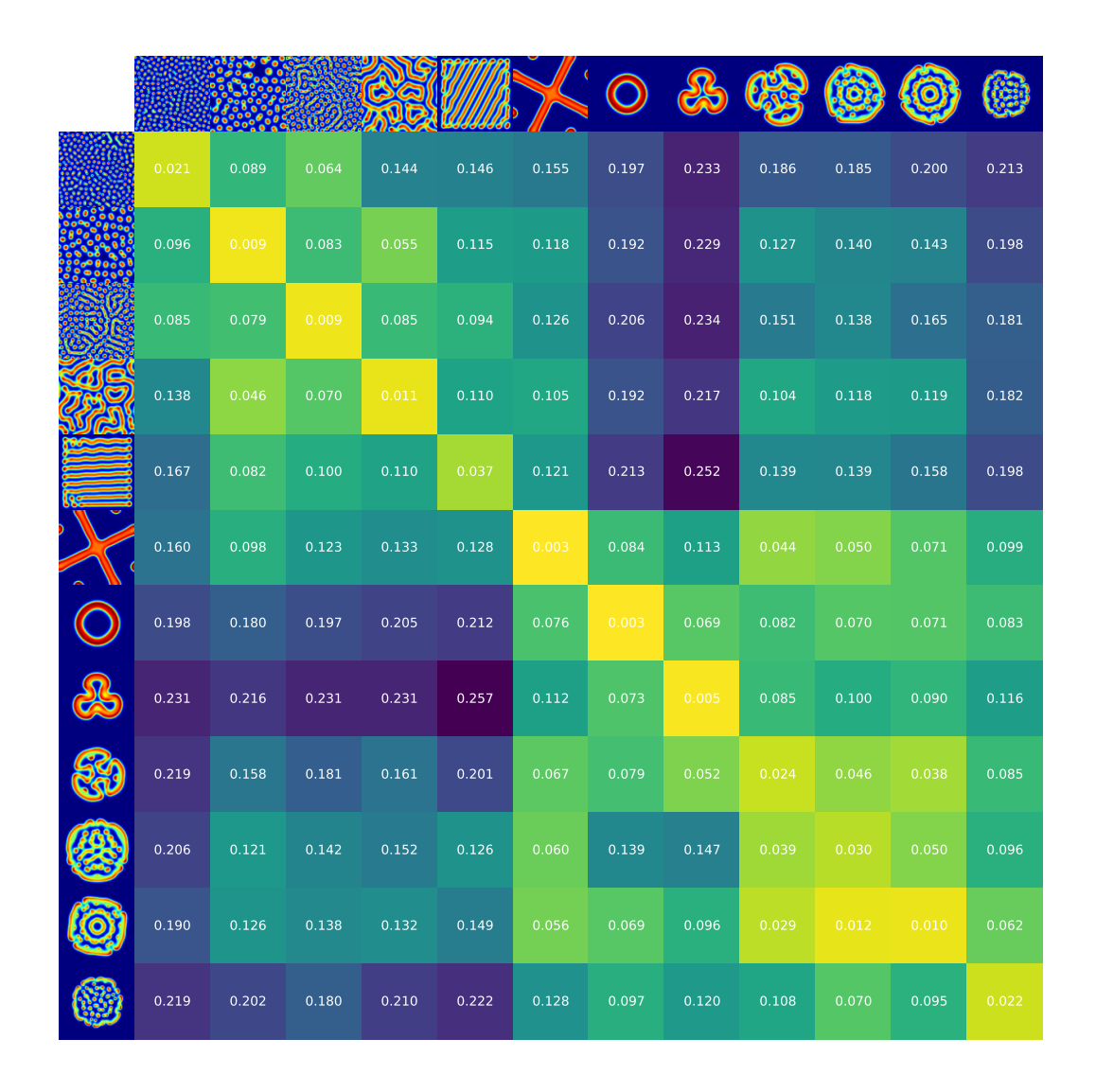


Figure 12: Embedding invariance across pattern instances of Gray-Scott model. Cosine distance matrix between CLIP embeddings of two sets of 12 patterns, Y and Y'. Each set of patterns is generated using the same set of parameters $\theta_i \in \Theta$ and a sampled initial configuration $s_0 \sim \mathcal{S}$. The inner matrix displays the pairwise cosine distances $1 - \cos(z_i, z_i')$ between the embeddings z_i and z_i' of patterns $y_i \in Y$ and $y_i' \in Y'$. The advantage of the invariant representation is evident in the high similarity (i.e., low cosine distance) along the diagonal, indicating that different pattern instances generated from the same causal parameter $\theta \in \Theta$ but different initial configuration $s_{0i} \sim S$ are represented closely together in embedding space.

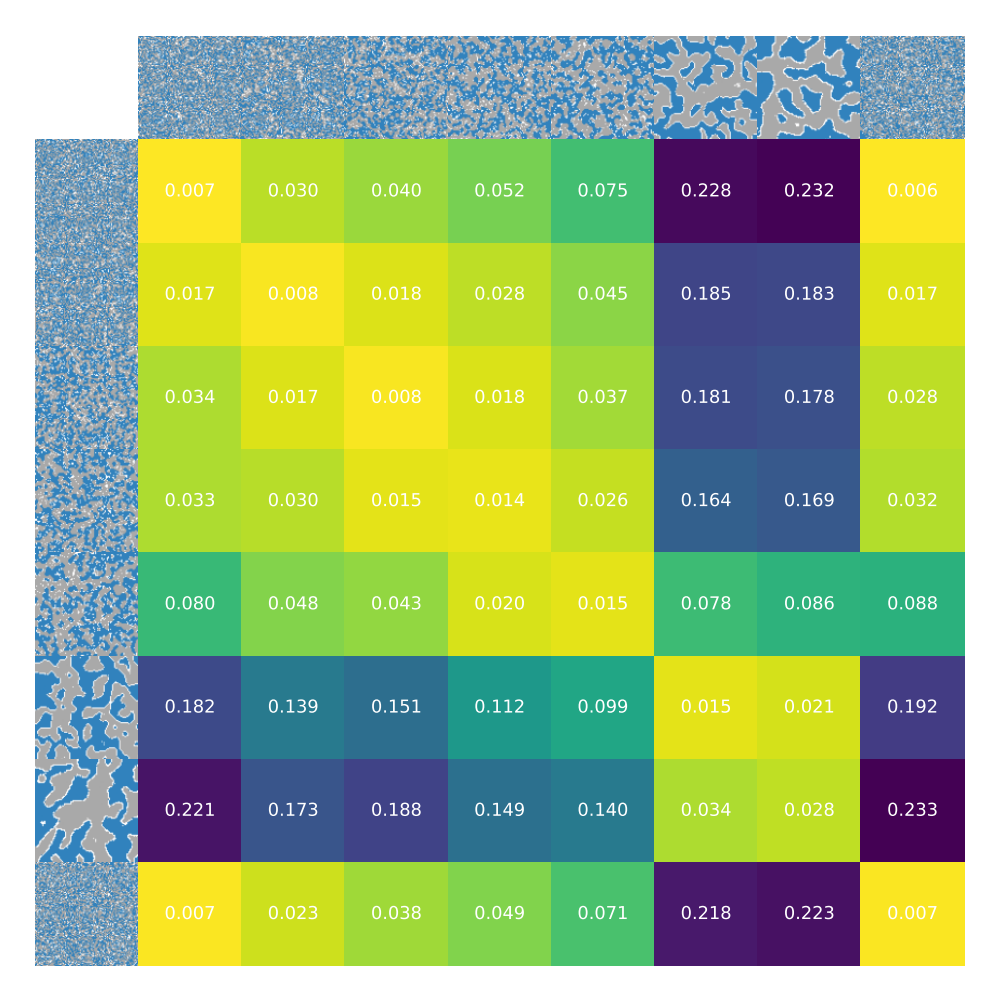


Figure 13: Embedding invariance across pattern instances of Schelling's model. Distance matrix between two different sets of 8 patterns, Y and Y'. Each set of patterns is generated using the same set of causal parameters Θ and different stochastic initial states S under the Schelling model. The inner matrix displays the pairwise cosine distances $1 - \cos(z_i, z_i')$ between the embeddings z_i and z_i' of patterns $y_i \in Y$ and $y_i' \in Y'$. As described in Figure 6, Schelling's model is non-injective and produces similar patterns y_i and y_i' for certain parameters, such as $\theta = T = 0.1$ and $\theta' = T' = 0.8$, a property reflected in both the observable space and the embedding distances.